24th INTERNATIONAL CONGRESS ON SOUND AND VIBRATION
23–27 July 2017, London

VORTEX PULSATION SIMULATION OF A PIPING NOISE DAMPENER

Georgy Makaryants

Samara National Research University, Faculty of Automatic Systems of Power Plants, Moskovskoe shosse st. 34, 443086 Samara, Russia
email: georgy.makaryants@gmail.com

This paper presents a research on dynamic characteristics of an internal pipe noise dampener. The study covers an investigation of vortex pulsations within a pipe system after the dampener. For this purpose, the numerical technique of estimation of hydrodynamic noise after the dampener diffuser has been developed. This technique is based on LES turbulence model. The obtained numerical data illustrates the inherent hydrodynamic noise level in the dampener diffuser. This noise level allows us to estimate background noise condition of the piping in which dampeners are used. The numerical results are verified by experimental data which confirm the adequacy of the developed model at the low frequency range.
Keywords: noise dampener, vortex, numerical simulation

1. Introduction

The study of oscillations in piping has become an important aspect of designing water supply and treatment systems. Water pressure pulsations induced by periodic flow after a pump and vortex shedding behind bends and changes in pipe cross-section are of particular interest and complexity. The pressure pulsations of working fluid may result in unacceptable level of pipeline vibration [1, 2] as well as in high acoustic noise [3, 4, 5, 7, 8]. One way around this problem is to use piping pressure pulsation dampeners [9 - 14]. In case of high flow rates a decisive role in dampener effectiveness and efficiency is the acoustic noise induced by vortex shedding downstream discontinuities encountered in dampener structure. One of such discontinuities is a diffuser connecting a dampener with a pipeline. Therefore, in order to solve the problem of dampener sound generation in a proper manner the process of vortex pulsation generation in the diffuser must be simulated.

The features of the flow passing through the diffuser have been widely discussed in the literature. There have been several investigations into the hydrodynamic processes inside the diffuser. McDonald & Fox [15] and then Kwong & Dowling [16] have demonstrated that a conical diffuser is affected by transitory stall. Dequand et al. [2] concluded that separation flow in the diffuser has significant influence on the formation of duct acoustic pulsations caused by vortex shedding. Kwong & Dowling [16] have described the flow field in the diffuser as stall cell. They have classified two modes of unsteadiness. In the first mode the upstream edge of the stall cell is exposed to oscillations with high tone amplitude. The second mode is associated with whole stall oscillations from one side of the diffuser to another. This kind of flow is characterized by broadband oscillations. Increased divergence angle of the diffuser leads to changes in the pulsation spectrum. First of all, the level of amplitudes considerably increases. Secondly, the spectrum becomes more broadband and the frequency of the tonal component reduces.

In the observed papers great attention is paid common phenomenon of the fluid passing through the diffuser. However, the methods and techniques of calculating the sound generation in piping components are also of particular interest. There is a several literature on this issue. One part of the

works is devoted to predict the vortex-born noise by means of semi-empirical techniques. For example Karekull et al. [5] put emphasis on searching for a general scaling law for the sound power for orifices, bends and dampeners. They used only the pressure drop derived from experiments or from simple steady-state calculation of fluid flow as an input parameters for modelling. The major benefit of this approach is the reduction of calculation time. In spite of this undeniable advantage, the method gives only an approximate level of the flow noise. Furthermore, the common grounds of the diffuser noise such as the presence of tonal spectrum component and the influence of divergence angle to spectral frequencies content cannot be conceptually modelled using the general scaling law. Unsteady Computational Fluid Dynamics (CFD) methods are used in the other part of the works in order to directly simulate the vortex sound generation, see, for example Lam et al. [6], Gloerfelt & Lafon [17], Singh & Rubini [13]. This approach allows us to obtain more detailed information on vortex noise. For example, Large Eddy Simulation (LES) technique applied to the flow in a diaphragm allowed Gloerfelt & Lafon [17] to demonstrate the ability of the Kelvin–Helmholtz vortices to dissipate wave propagation. Although considerable research has been devoted to direct computation of the duct noise radiated by a vortex flows issuing from any diaphragms, abrupt expansions and duct junctions, rather less attention has been paid to CFD calculation of turbulent flows in a diffuser. Furthermore, there are few studies devoted to the investigation of mesh resolution impact on direct computation hydrodynamic noise.

The aim of this paper is to extend the use of unsteady CFD methods in order to simulate vortex pulsations appearing downstream of the diffuser as well as to find vortex noise inside the duct.

2. Operation principle of a piping noise dampener

The piping noise dampener consists of a non-flowing vessel placed parallel to a constricted duct that passes the mean flow (Fig. 1). In high frequency range the vessel has a significant acoustic conductivity while the constricted duct poses a high acoustic resistance. That is why in high frequencies the flow oscillation energy is isolated inside the non-flowing vessel and it does not passed through the dampener. Isolated oscillation energy is attenuated in hydraulic throttles connected the constricted duct and the non-flowing vessel. In terms of the electroacoustic analogies theory a vessel and a duct are reactive wave resistances and a hydraulic throttle is an active one. Herewith, for the maximum acoustic wave absorption the wave impedance of the dampener and connected pipeline must be equal each other. While the wave impedance of the pipeline is frequency independent and active the hydraulic throttle must provide the similar character of wave resistant in the inlet and outlet of the dampener. Therefore, this type of dampener is called the dampener with constant active resistance [12].

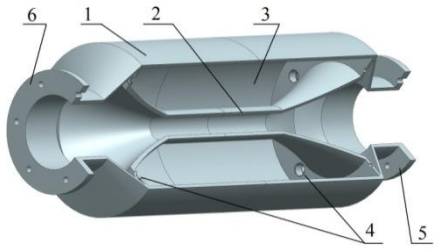

Figure 1: Schematic representation of the dampener. (1) Dampener housing assembly. (2) Constricted duct. (3) Non-flowing vessel. (4) Hydraulic throttles. (5), (6) Connecting flange.

3. Methods

The process of the vortex pulsation modelling consisted of two stages. The first stage was devoted to the flow analysis using steady-state Reynolds-averaged Navier-Stokes (RANS) model. During this calculation the low-Reynolds $k-\omega SST$ turbulence model was used to closure governing equations. The choice of such turbulence model was made due to its best ability to predict the

flow separation from the wall [18]. The results of steady-state calculation defined the mesh size as well as the initial conditions to the flow analysis using LES that carried out at the second stage. Finally the acoustic pulsation was evaluated in the region with the maximum distance from the diffuser. Fig. 2 depicts the geometry of flow domain region.

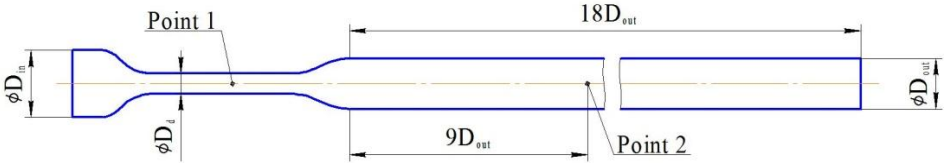

Figure 2: Geometry of computational domain.

3.1 Governing equations

The prediction of pressure pulsations in the diffuser as well as their propagation need the calculation of the flow parameters time dependency. For this purpose it is necessary to solve the complete system of hydrodynamics equations in three-dimensional form. This system consists of the continuity equation:

$$\frac{\partial \rho}{\partial t} + \frac{\partial \rho u_j}{\partial x_j} = 0, \tag{1}$$

and the momentum equation

$$\frac{\partial \rho u_i}{\partial t} + \frac{\partial \rho u_j u_i}{\partial x_j} = -\frac{\partial p}{\partial x_i} + \frac{\partial \tau_{ij}}{\partial x_i}, \tag{2}$$

where ρ is a density, u_j and x_j ($j = 1,2,3$) is a velocity and a displacement projection on the axis of a Cartesian system, p is a pressure, τ_{ij} is components of stress tensor, t is a time. The repeated index convention for summation is systematically used. Moreover, the complete system of hydrodynamics equations also includes the state equation. However, the accepted assumption that the wave processes are adiabatic made it possible to eliminate the temperature from the state equation. This led to the relation between density and pressure using Tait equation of state

$$\rho = \rho_0 \sqrt[n]{\frac{K_0 + n\Delta p}{K_0}}, \tag{3}$$

where ρ_0 is a reference liquid density, K_0 is a reference bulk modulus, n is a density exponent, $\Delta p = p - p_0$, p is an absolute liquid pressure, p_0 is an absolute reference liquid pressure.

The solution of the system of hydrodynamics equations was carried out using their LES filtering. Then the filtered of the continuity equation is written as

$$\frac{\partial \bar{\rho}}{\partial t} + \frac{\partial \bar{\rho} \tilde{u}_j}{\partial x_j} = 0, \tag{4}$$

where $\bar{\rho}$ is LES-filtered density, $\tilde{u}_j$ is the Favre-filtered velocity. The filtered momentum equation is written as

$$\frac{\partial \bar{\rho} \tilde{u}_i}{\partial t} + \frac{\partial \bar{\rho} \tilde{u}_j \tilde{u}_i}{\partial x_j} = -\frac{\partial}{\partial x_i}\left(\bar{p} + \frac{2}{3}\mu \frac{\partial \tilde{u}_k}{\partial x_k}\right) + \frac{\partial}{\partial x_i}\mu\left(\left(\frac{\partial \tilde{u}_i}{\partial x_j} + \frac{\partial \tilde{u}_j}{\partial x_i}\right) - \bar{\rho}\tau_{ij}^r\right), \tag{5}$$

where $\bar{p}$ is LES-filtered pressure, $\tau_{ij}^{r} = \tilde{u_j u_i} - \tilde{u}_j \tilde{u}_i$ is a residual stress tensor, μ is a dynamic viscosity. The residual stress tensor is derived from the following expression

$$\tau_{ij}^{r} = -2\nu_{SGS} S_{ij}, \tag{6}$$

where $S_{ij} = 1/2\left(\partial \tilde{u}_i / \partial x_j + \partial \tilde{u}_j / \partial x_i \right)$ is a rate-of-strain tensor, ν_{SGS} is an eddy viscosity. The eddy viscosity was calculated by taking into account the influence of the pipe wall to the fluid flux. For this purpose the wall-adapting local eddy-viscosity (WALE) model was used. According to Nicoud and Ducros [19] in the WALE model the eddy viscosity is computed by

$$\nu_{SGS} = \left(0.325 V^{1/3}\right)^2 \frac{\left(S_{ij}^{d} S_{ij}^{d}\right)^{3/2}}{\left(S_{ij} S_{ij}\right)^{5/2} + \left(S_{ij}^{d} S_{ij}^{d}\right)^{5/4}}, \tag{7}$$

where $S_{ij}^{d} = 1/2\left(\left(\partial \tilde{u}_i / \partial x_j \right)^2 + \left(\partial \tilde{u}_j / \partial x_i \right)^2 \right) - 1/3 \delta_{ij} \left(\partial \tilde{u}_k / \partial x_k \right)^2$, V is the cell volume.

The system of hydrodynamics equations was computed using a finite volume method with pressure-based solver and pressure-velocity coupled scheme, using the FluentCFD-14.5 code. Therewith, the cell size and the time step of the flow simulation will be defined thoroughly due to their high influence to the computational accuracy.

3.2 Space and time discretization

The estimation of fluid pulsations caused by vortex shedding downstream the diffuser was carried out using LES analysis. When it comes to the computational accuracy of vortex structure and vortex induced acoustic waves the main simulating parameter is cells size. Since it is the cells size that determines the computational ability to explicitly model the vortex structures. The following two factors influences to the cells size determination. The first factor related to minimum cells size, it suggests that for the vortex prediction it is required smaller cells size than for acoustic computation. In this case, the cells size is determined in accordance with the minimum scale of energy contented vortex. The second factor relates to the cells size distribution in computational domain. The computational domain have to be sufficiently large. This is due to the need to separate the vortex pulsations from the acoustic waves. This separation can be performed by registering the parameters of pulsations far from the diffuser, where the vortex structures are damped due to the decay process. The employment of the minimum cells size throughout the computational domain demands the impossibly large computational requirements. This problem was solved by increasing cells size with distance from the diffuser. It becomes possible in connection with the magnification of the energy contented vortex scale due to vortex decay. Hence, the calculation of the energy contented vortex scale distribution by the length of the computational domain diminished demands to the cells size. The energy contented vortex scale can be estimated using RANS model as follows

$$L_{\varepsilon} = \frac{k^{3/2}}{\varepsilon}, \tag{8}$$

where k is the kinetic energy of turbulence, ε is the dissipation rate of the turbulence kinetic energy. In this case, the value of the linear cell size is chosen equal to one eighth magnitude of the obtained scale. This let to use of eight cells to calculate the large vortex, which is the minimum for an explicit simulation of the vortex structure. This was the way to select the cell size in the core of the flow.

The other no less important aspect was the computation of the vortex onset result from detaching the flow from the wall. Hence, a particular attention was paid to establish the cells size in near-wall region. For its explicit modeling, the height of the first cell should not exceed the height of the viscous sublayer. To satisfy this condition, the dimensionless distance to the wall y^+ must be less than or equal to one. Hence, according to Pope [20] the height of the first mesh layer attached to wall is given by

$$\Delta y \le \frac{\mu}{\rho}\left[\left(2\cdot log_{10}\,Re - 0{,}65\right)^{-2{,}3} u^2\, 0{,}5\right]^{-0{,}5}, \tag{9}$$

where μ is dynamic viscosity of the fluid; ρ is the fluid density; u is fluid velocity away from the boundary layer, and Re is the Reynolds number. By moving out the wall, the mesh size increased in 1.2 times. The size of the near-wall region is estimated from the boundary layer displacement thickness [21].

$$\delta^* = \frac{d/2}{1+1{,}5\,lg\left(Re\right)}, \tag{10}$$

where d is the inner diameter of the piping, Re is the Reynolds number. The time step value selection was based on the required maximum frequency in the spectrum of vortex pulsations:

$$\Delta t = \frac{1}{2\,f_{max}}. \tag{11}$$

3.3 Boundary conditions

As a boundary condition at the input, a constant total pressure of the fluid was set. At the output, a constant flow rate was set. This made it possible not only to determine the hydrodynamic flow conditions, but also to set the conditions for the behavior of the acoustic wave reaching the output section. Constant flow means that its pulsation component is equal to zero, which leads to the fact that the impedance of the hydraulic load connected to the output section tends to infinity. In other words, from the acoustic point of view, setting the output at a constant flow rate, the conditions for the acoustically closed end were set. This was result in the appearance of a standing wave corresponding to the quarter-wave resonance of the fluid column located behind the diffuser. The frequency of the quarter-wave resonance can be estimated follows:

$$f_{rez} = \frac{a}{4l}. \tag{12}$$

where a is the sound velocity, l is the length of the fluid column located behind the diffuser. Further, the resulting resonant peak was not taken into account in the spectrum of pulsations caused by the vortex structures. To exclude the influence of the output boundary condition on the formation of vortex structures [22-24], their propagation and decay, the output section of the calculated region was removed from the diffuser by the length of 18 outlet diffuser diameters.

4. Results and discussions

4.1 Results of RANS modelling

In what follows, the results of the pilot study in flow dynamics passed through the diffuser are described. Fig. 3 depicts the results of flow velocity computing in the near-wall region. The dimensionless data were showed for the crossection with the minimum diameter of the fluid domain (Fig 2, point 1). As can be seen, the minimum value of the dimensionless wall distance y^+ was 0.5. The achieved y^+ was less than one, this being proving an adequate calculation of the first near-wall

cell height for explicitly computation of the viscous sublayer. Moreover, the graph clearly illustrates viscous sublayer, blending region, log-law region and outer layer, this being demonstrating an appropriate cells density for the explicit estimation of the near-wall region.

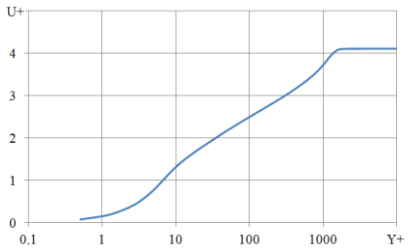

Figure 3: Dimensionless flow velocity in the near-wall region (point 1).

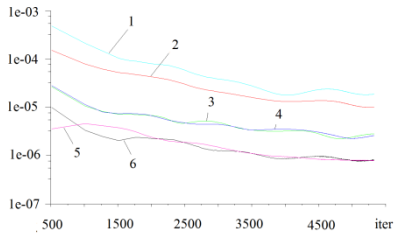

Figure 4: Computational residuals of RANS modelling. (1) k, (2) x-velocity, (3) y-velocity, (4) z-velocity, (5) omega, (6) continuity.

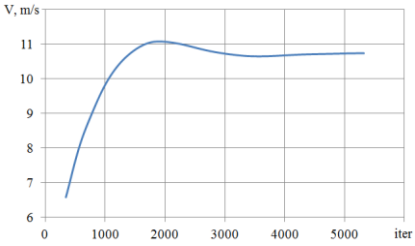

Figure 5: Mean flow velocity evolution versus the iterations (point 1).

Then, the number of iterations required for mean flow estimation was selected. Fig. 4 illustrates the stabilization of computational residuals on appropriate level of 10^{-4} – 10^{-6} after 5 000 iterations. The other factor that indicated the convergence of mean-flow computation was the estimation of mean flow velocity at duct benchmark points. Fig. 5 shows the mean flow velocity evolution versus the iterations at point 1. As can be seen, the value of the velocity stabilizes over the 10.5 m/s, that is adequate to its approximate estimation from the balance of flow rate.

Hence, the results of mean flow analysis is believed to be adequate. In what follows, the evaluated data (Fig. 6 a, b) were used as initial conditions for the transient flow analysis. Moreover, the obtained results and the equation (8) were used to estimate the distribution of energy contented vortex scale over the computational domain (Fig. 6 c). This scale was used to adopted computational mesh for transient LES simulation.

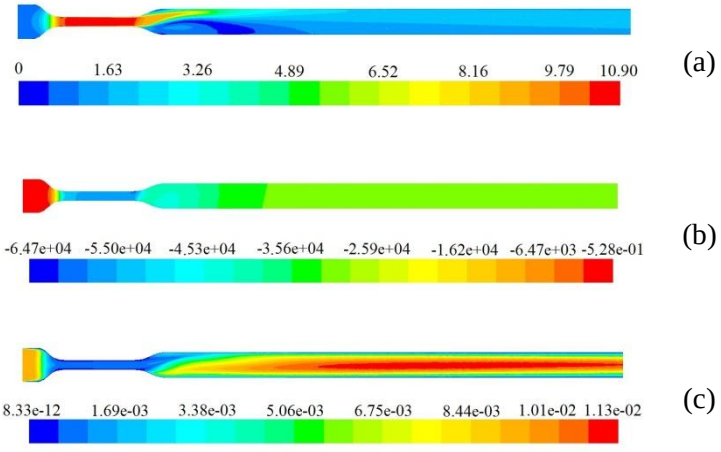

Figure 6: Reynolds averaged flow parameters distributions. (a) Flow velocity. (b) Flow static pressure. (c) Energy contented vortex scale.

4.2 Results of LES modelling

The flow at the diffuser outlet was showed to be unstable according to instantaneous velocity field in longitudinal section (Fig. 7). The alternation of the flow parts with positive and negative axial velocity component indicated the periodicity of flow separation from the wall process. Fig. 8 depicts the root-mean-square pressure pulsation field. The flow zone with the maximum value of velocity pulsation was observed inside the diffuser. At the axial direction, this zone propagated throughout the length of the diffuser. At the radial direction, this zone located by the diameter of the

diffuser inlet section. The vortex pulsation illustrated to arise in the inlet of the diffuser and along its wall.

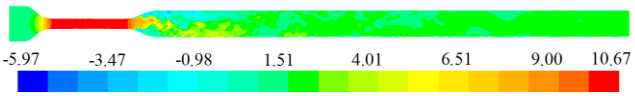

Figure 7: Snapshot of the instantaneous velocity.

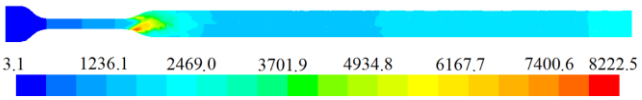

Figure 8: RMS pressure pulsation distribution.

The pressure time history data was collected at the axial duct point (Fig. 2 point 2) at a distance of nine diffuser outlet diameters. Fig. 9 compares the third-octave spectra of estimated theoretical results and experimental data obtained previously [25]. It should be noted that the acceptable coincidence of theoretical and experimental spectra was achieved up to a frequency of 8 Hz. However, above the frequency of 8 Hz the theoretical spectrum unfortunately became lower than experimental one. Presumably, the lack of coincidence at the frequency rage over 8 Hz was suggested to be associated with insufficient time step used for prediction of high frequency flow dynamics.

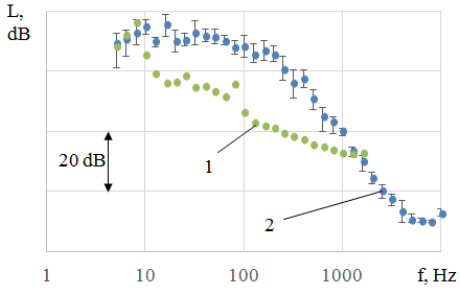

Figure 9: Spectrum of inherent hydrodynamic noise level. (1) Theoretical data. (2) Experimental data.

5. Conclusion

A direct vortex borne noise computation in liquid fluid passed through the diffuser was obtained. It was noted that the source of the vortex pulsations located in the inlet of the diffuser along its wall. An acceptable coincidence of theoretical and experimental results was achieved at the frequencies up to 8 Hz. A vortex borne nose simulation accuracy increase can be carry out by decreasing the time step of transient flow analysis.

6. Acknowledgments

This work was supported by the Ministry of Education and Science of the Russian Federation.

REFERENCES

1 Tian, J., Yuan, Ch., Yang, L., Wu, Ch., Liu, G. and Videa, Zh. The vibration analysis model of pipeline under the action of gas pressure pulsation coupling, *Engineering Failure Analysis*, **66**, 328–340, (2016).

2 Dequand, S., van Lier, L., Hirschberg, A. and Huijnen, J. Aeroacoustic response of diffusers and bends: comparison of experiments with quasi-steady incompressible flow models, *Journal of Fluids and Structures*, **16** (7), 957–969, (2002).

3 Musaakhunova, L.F., Igolkin, A.A., and Shabanov, K.Y. The vibroacoustic characteristics research of the gas pipeline, *Procedia Engineering*, **106**, 316–324, (2015).

4 Igolkin, A.A., Musaakhunova, L.F. and Shabanov, K.Y. Method development of the vibroacoustic characteristics calculation of the gas distribution stations elements, *Procedia Engineering*, **106**, 309–315, (2015).

5 Kårekull, O., Efraimsson, G. and Åbom, M. Prediction model of flow duct constriction noise, *Applied Acoustics*, **82**, 45–52, (2014).

6 Lam, G.C.Y., Leung, R.C.K and Tang, S.K. Aeroacoustics of duct junction flows merging at different angles, *Journal of Sound and Vibration*, **333** (18), 4187–4202, (2014).

7 Gafurov, S., Rodionov, L., and Makaryants, G. Simulation of gear pump noise generation, *Proceedings of the 9th FPNI Ph.D. Symposium on Fluid Power, FPNI 2016*, Florianópolis, Brazil, 26–28 October, (2016), doi:10.1115/FPNI2016-1531.

8 Rodionov, L., and Rekadze, P. Exploration of acoustic characteristics of gear pumps with polymeric pinion shafts, *Procedia Engineering*, **106**, 36–45, (2015), doi:10.1016/j.proeng.2015.06.006.

9 Shorin, V.P. and Sanchugov, V.I. On estimating the operating efficiency of suppressors of liquid pulsations, which contain resonant loops in their structure, *Power Eng (New York)*, **16** (2), 113–120, (1978).

10 Ermilov, M.A., Kryuchkov, A.N., Balyaba, M.V. and Shabanov, K.U. Development of a Pressure Pulsation Damper for Gas Pressure Regulators with Account of Operation Parameters, *Procedia Engineering*, **106**, 277-283, (2015), doi: 10.1016/j.proeng.2015.06.036.

11 Ermilov, M.A., Balyaba, M.V., Kryuchkov, A.N., and Shabanov, K.Y. The experimental development of the pulsation damper in a gas reduction line, *Proceedings of the 22 International Congress on Sound and Vibration*, Florence, Italy, 12–16 July, (2015).

12 Golovin, A.N., and Shorin, V.P. Designing fluid-oscillation dampers, *Power Eng (New York)*, **20** (4), 132–138, (1982).

13 Singh, N.K., and Rubini, P.A. Large eddy simulation of acoustic pulse propagation and turbulent flow interaction in expansion mufflers, *Applied Acoustics*, **98**, 6–19, (2015).

14 Xiwen Dai Vortex convection in the flow-excited Helmholtz resonator, *Journal of Sound and Vibration*, **370**, 82–93, (2016).

15 McDonald, A.T. and Fox, R.W. An experimental investigation of incompressible flow in conical diffusers, *International Journal of Mechanical Sciences*, **8** (2), 125–130, (1966).

16 Kwong, A.H.M. and Dowling, A.P. Unsteady flow in diffusers, *Journal of Fluids Engineering, Transactions of the ASME*, **116** (4), 842–847, (1994).

17 Gloerfelt, X. and Lafon, P. Direct computation of the noise induced by a turbulent flow through a diaphragm in a duct at low mach number, *Computers and Fluids*, **37** (4), 388-401, (2008).

18 Menter, F.R. and Sarkar, S. Two-equation eddy-viscosity turbulence models for engineering applications, *AIAA Journal*, **32** (8), 1598-1605, (1994).

19 Nicoud, F., and Ducros, F. Subgrid-scale stress modelling based on the square of the velocity gradient tensor, *Flow, Turbulence and Combustion*, **62** (3), 183-200, (1999).

20 Pope, S., *Turbulent Flows*, Cambridge Univ. Press., Cambridge (2000).

21 Smol'yakov, A. V. Noise of a turbulent boundary layer flow over smooth and rough plates at low mach numbers, *Acoustical Physics*, **47** (2), 218-225, (2001).

22 Gullman-Strand, J., Tornblom, O., Lindgren, B., Amberg, G., and Johansson, A.V. Numerical and experimental study of separated flow in a plane asymmetric diffuser, *International Journal of Heat and Fluid Flow*, **25**, 451-460, (2004).

23 Wallin, S. and Johansson, A.V. An explicit algebraic Reynolds stress model for incompressible and compressible turbulent flows, *Journal of Fluid Mechanics*, **403**, 89-132, (2000).

24 Jakirlic, S., Kadavelil, G., Kornhaas, M., Schafer, M., Sternel, D.C. and Tropea, C. Numerical and physical aspects in LES and hybrid LES/RANS of turbulent flow separation in a 3-D diffuser, *International Journal of Heat and Fluid Flow*, **31**, 820-832, (2010).

25 Makaryants, G.M., Gafurov, S.A., Zubrilin, I.A., Kruchkov, A.N., Prokofiev, A.B., and Shakhmatov, E.V. Design methodology of hydrodynamic noise silencer, *Proceedings of the 20th International Congress on Sound and Vibration*, Bangkok, Tailand, 7–11 July, (2013).